PROCEEDINGS, Thirty-Fifth Workshop on Geothermal Reservoir Engineering
Stanford University, Stanford, California, February 1-3, 2010
SGP-TR-188

IN-SITU STRESS AND FRACTURE CHARACTERIZATION FOR PLANNING OF AN EGS STIMULATION IN THE DESERT PEAK GEOTHERMAL FIELD, NEVADA

Stephen H. Hickman[1] and Nicholas C. Davatzes[2]

[1]U.S. Geological Survey
345 Middlefield Road, MS977
Menlo Park, CA 94025, USA
e-mail: hickman@usgs.gov

[2]Temple University
EES, 1901 N. 13th St
Philadelphia, PA, 19122, USA
e-mail: davatzes@temple.edu

ABSTRACT

An integrated study of natural fracture geometry, fluid flow and stress was conducted in Desert Peak well 27-15 in preparation for development of an Enhanced Geothermal System (EGS) through hydraulic stimulation. This stimulation will be carried out at depths of ~3000 to 3500 ft in units comprised of silicified rhyolite tuffs and metamorphosed mudstones at ambient temperatures of ~180 to 195° C. Our previous analyses of borehole image logs from this well showed that the current minimum horizontal principal stress, S_{hmin}, is oriented 114 ± 17º and that numerous fractures in the planned stimulation interval are optimally oriented for normal faulting. As an extension of this earlier work, a hydraulic fracturing stress measurement was conducted at the top of the intended stimulation interval and indicates that the magnitude of S_{hmin} is 1995 ± 60 psi, which is ~0.61 of the calculated vertical (overburden) stress at this depth. This S_{hmin} magnitude is somewhat higher than expected for frictional failure on optimally oriented normal faults under current reservoir pressures given typical laboratory measurements of sliding friction (Byerlee's Law). However, Coulomb failure calculations using coefficients of friction derived from laboratory tests on representative core samples from a nearby well (Lutz et al., 2010) indicate that shear failure could be induced on well-oriented pre-existing fractures in well 27-15 once fluid pressures are increased by several hundred psi above the ambient formation fluid pressure. This geomechanical model will be tested during hydraulic stimulation of well 27-15, which is intended to enhance formation permeability through self-propping shear failure. If this stimulation is successful, then preferential activation of normal faults should generate a zone of enhanced permeability propagating to the SSW, in the direction of nearby geothermal injection and production wells, and to the NNE, into an unexploited portion of the field.

1. INTRODUCTION

Characterization of the geometrical and hydrologic properties of natural fractures in relation to the *in-situ* state of stress is critical to the planning and evaluation of hydraulic stimulations carried out in Enhanced Geothermal Systems (EGS) projects (MIT, 2006). Studies in a variety of tectonic settings have shown that fractures which are optimally oriented and critically stressed for frictional failure often dominate fluid flow in low-porosity crystalline rocks (Barton, 1995; Ito and Zoback, 2000; Townend and Zoback, 2000). Similar studies in a high-temperature fault-hosted geothermal system at Dixie Valley, Nevada (Barton et al., 1998; Hickman et al., 1998, 2000) indicate that actively slipping (i.e., shearing) fractures help maintain geothermal reservoir permeability despite crack sealing and other geochemical fluid-rock interactions that should destroy that permeability.

By analogy to these natural case studies, the goal of EGS hydraulic stimulations is to artificially induce shear slip and dilatation along pre-existing fractures by injecting fluids at low pressures (preferably below the least principal stress), thereby enhancing formation permeability in hot but impermeable rocks. For these stimulations to be successful, the targeted formations should contain slightly permeable natural fractures that are well oriented and highly stressed for shear failure and have the appropriate mechanical properties for the generation and maintenance of shear-enhanced fracture dilatation.

In this paper we present recent results from ongoing characterization of fracturing and stress state in Desert Peak well 27-15, which has been selected for EGS stimulation and is located immediately north of the currently producing reservoir for the Desert Peak Geothermal Field (Figure 1). Three depth intervals in well 27-15 were considered for stimulation: 1) stimulate just below the casing shoe at depths of 3000 to 3500 ft, 2) recomplete the well and stimulate at

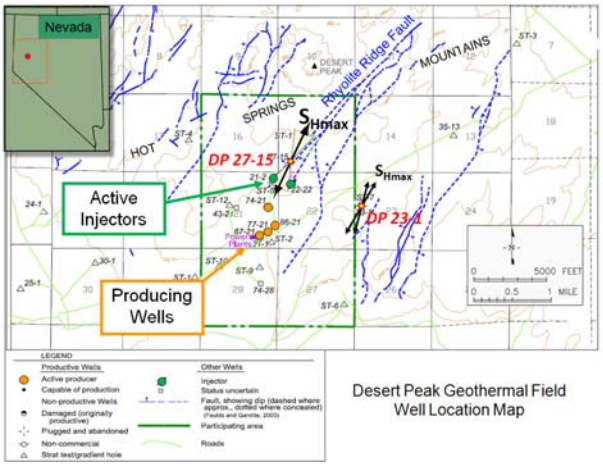

Figure 1: Map of the Desert Peak Geothermal Field, showing EGS well 27-15 and active injecting and producing wells. Fault traces (shown in blue) were mapped by Faulds and Garside (2003). Orientations of the maximum horizontal principal stress, S_{Hmax}, were inferred from observations of borehole failure in wells 27-15 and 23-1 by Davatzes and Hickman (2009) and Robertson-Tait et al. (2004), respectively.

4500 to 5000 ft, or 3) side-track around a lost bottom-hole assembly, recomplete and stimulate at 5300 to ~6500 ft. Although all three intervals have advantages and disadvantages, the shallowest interval was selected for stimulation primarily because it offered the best chance for connecting to the producing part of the Desert Peak Geothermal Field through the rhyolite units associated with the main producing horizon (see discussion in Zemach et al., 2009). Other advantages of targeting the shallow interval were that rock strength could be determined using core from the same lithologic units in nearby well 35-13 (see Figure 1) and that additional stimulations could still be conducted at a later date in the deeper zones. Well 27-15 was recompleted in July 2009, leaving an open-hole stimulation interval extending from the casing shoe at 3013 ft below ground level (GL) to the top of a cement plug at 3474 ft GL. A summary of the lithology and mineralogy of rocks in the well 27-15 stimulation interval based upon cuttings analysis and results from mechanical testing on cores from well 35-13 is presented in Lutz et al. (2010).

During the first phase of our study (Davatzes and Hickman, 2009) we analyzed stress orientations and fracture characteristics in all three potential stimulation intervals of well 27-15. This included analysis of electrical and acoustic image logs for the orientation and depth distribution of natural fractures, bedding/foliation and stress-induced borehole failure, and analysis of temperature/pressure/spinner (TPS) logs to reveal fluid entry/exit points. In the present paper, we extend this earlier work by using a new small-volume hydraulic fracturing stress test (minifrac) conducted during recompletion of well 27-15 to generate a 3-D stress model. We then use this model together with fracture orientations determined from the image logs and rock friction measurements made on core from well 35-13 to predict fluid pressures necessary to induce shear failure on pre-existing fractures within the stimulation interval. We then discuss the implications of this analysis for the planned EGS stimulation of well 27-15.

2. RESULTS

2.1 Hydraulic Fracturing Stress Measurement

A small-volume, low-flow-rate hydraulic fracturing test (minifrac) was conducted in July 2009 in an open-hole interval of well 27-15 at depths of 3013 to 3095 ft GL, between the casing shoe and the top of a temporary cement plug. Following the minifrac, this cement plug and underlying sand were drilled out to the top of another cement plug, which forms the base of the planned stimulation interval.

As done in other geothermal wells (e..g, Hickman et al., 1998, 2000; Davatzes and Hickman, 2006), after the hole was cleaned out to the top of the cement plug, a drill-pipe-deployed packer (RTTS tool) was set in the cased hole at a depth of 2889 ft GL. The wellhead blow-out preventer was then closed around the drill pipe and the annular pressure between the casing and drill pipe raised to a few hundred psi to allow monitoring of "back side" pressure on the RTTS. (This allowed us to confirm that the RTTS maintained a good seal against the casing and that there was no packer bypass during the minifrac.) During the first cycle of the minifrac, the drill pipe was pressurized at a flow rate of 1 bbl/min to induce a hydraulic fracture in the uncased test interval. Subsequently, repeated fluid injection (at 2 bbl/min) and flowback cycles were then employed to extend this fracture away from the borehole (Figure 2a). Test pressure was measured downhole using a high-accuracy, temperature-compensated quartz pressure gauge suspended just below the RTTS at a depth of 2992 ft GL. Flow rate into and out of the well was monitored at the surface using turbine flow meters, calibrated before the minifrac against timed discharge from a known volume. Fresh water and dilute formation brine were used throughout the test to minimize viscous pressure losses.

Following Hickman and Zoback (1983) and Hickman et al. (1988), the magnitude of S_{hmin} was determined from the stable instantaneous shut-in pressure (ISIP) obtained during multiple fracture propagation cycles, where ISIP is the pressure at which the pressure-time curve departs from an initial linear pressure drop immediately after the pump is turned off and the well

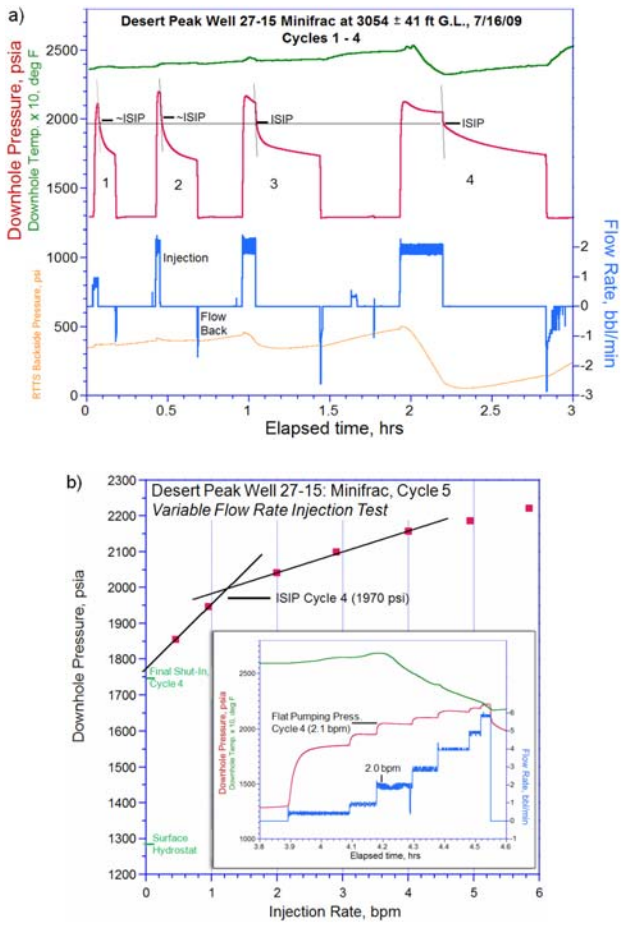

Figure 2: a) Pressure and flow rate records from the small-volume hydraulic fracturing (minifrac) test conducted in well 27-15 just below the casing shoe at 3013 to 3095 ft below ground level (GL). Downhole pressure and temperature were recorded using a quartz pressure/temperature tool suspended at a depth of 2992 ft GL; therefore, in this figure and in Figure 2b, add 25 psi to correct pressures shown to test interval center. Also shown in gold is the RTTS backside pressure, which confirmed packer seal integrity during this test. b) Variable flow-rate injection test (inset) conducted at the conclusion of the minifrac. Also shown are long-term shut-in pressure at the end of cycle 4 and the surface hydrostatic pressure between minifrac cycles.

is shut in (Figure 2a). Importantly, the ISIP was quite distinct in the fourth cycle of the test following pumping at 2 bbl/min (1970 psi) and is consistent with the ISIPs obtained earlier in the test, including in the first cycle after pumping at 1 bbl/min (~1992 psi). As discussed in Hickman and Zoback (1983) and Hickman et al. (1988), this shows that viscous pressures losses within the hydraulic fracture near the borehole were small, as expected for these low flow rates and low fluid viscosities, and that the stable ISIP provides a reliable measure of S_{hmin}. Since the downhole pressure recorder was located 62 ft above the test interval center, pressures in Figure 2 were extrapolated to test interval center using the measured bottom-hole fluid pressure gradient. In this manner and using the cycle 4 ISIP, we determined that the magnitude of S_{hmin} at 3054 ± 41 ft GL (covering the entire open-hole test interval) is 1995 ± 60 psi.

Downhole pumping pressures recoded during a step-wise increase in flow rate at the end of the minifrac (Figure 2b) were used to independently constrain the magnitude of S_{hmin}. As discussed in Zoback (2007, p. 216), plots of excess pressure against injection rate should exhibit a decrease in slope once S_{hmin} is exceeded and the hydraulic fracture re-opens at some distance from the borehole. For the variable flow-rate injection test from well 27-15, the inflection point so indicated is very close to the stable ISIP obtained at the end of cycle 4 (Figure 2b), corroborating the magnitude of S_{hmin} as determined from the minifrac.

In our analysis, one principal stress is assumed to be vertical and equal to the overburden, S_V (see rationale in Hickman, 1991). Since no open-hole geophysical density logs were run in well 27-15 above 3013 ft GL, S_V was calculated from a detailed lithologic profile derived from cuttings analysis performed during drilling of well 27-15 together with densities measured on core of the same rock types from well 35-13. In this manner, we calculated that S_V at the test interval center (3054 ft GL) is ~3277 psi, so that S_{hmin}/S_V ~0.61. To estimate the ambient formation fluid pressure, P_P, we used an equilibrated TPS survey conducted in well 27-15 on September 7, 2006, when the borehole was filled with formation fluid and had been shut-in for several years. At this time, the static fluid level in well 27-15 was at 380 ft GL, which is our best estimate for the current, undisturbed water table for the open-hole interval. The depth variations in S_V and ambient P_P calculated for well 27-15, along with the measured magnitude of S_{hmin} from the minifrac, are shown in Figure 3.

It is interesting to compare S_{hmin} as determined from the minifrac test with limits on differential stress in the crust imposed by frictional faulting theory and laboratory friction measurements (e.g., Townend and Zoback, 2000). According to the Coulomb failure criterion, frictional failure (i.e., normal faulting) would be expected to occur on optimally oriented, cohesionless normal faults at a critical magnitude of S_{hmin} given by (Jaeger and Cook, 1976):

$$S_{hmin\ crit} = (S_V - P_P) / [(\mu^2 + 1)^{1/2} + \mu]^2 + P_P \qquad (1)$$

where μ is the coefficient of friction of preexisting fractures. In applying Equation 1 it is assumed that μ ranges from 0.6 to 1.0, as observed in laboratory sliding experiments on a variety of standard rock

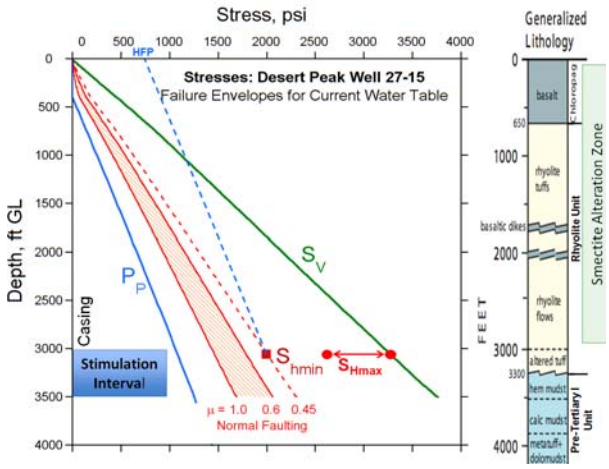

Figure 3: Magnitude of the least horizontal principal stress, S_{himn}, from the minifrac in well 27-15. The vertical stress, S_V, and formation fluid pressure, P_p, were calculated as described in the text. The dashed lines indicate the range of S_{himn} at which frictional failure would be expected on optimally oriented normal faults for coefficients of friction, μ, ranging from 0.6 to 1.0. The dashed blue line is the borehole pressure (at ambient formation temperatures and fluid densities) at which a hydraulic fracture should start to propagate at the top of the planned EGS stimulation interval, corresponding to a wellhead hydrofrac pressure (HFP) of ~750 psi. The generalized lithologic profile is from analysis of drill cuttings by Lutz et al. (2009).

types (Byerlee, 1978). In this manner, we calculated the range of S_{hmin} magnitudes at which normal faulting would be expected along optimally oriented normal faults for the current, undisturbed water table (Figure 3). As the measured value for S_{hmin} falls above the μ = 0.6 failure line, it appears that differential stress (i.e., S_V - S_{hmin}) in the stimulation interval is not low enough to lead to frictional failure under ambient fluid pressure conditions. However, illite and other clays were observed in analyses of drill cuttings from the well 27-15 stimulation interval (Lutz et al., 2010). Since μ ~0.45 for illite (Lockner and Beeler, 2002), it is possible that frictional failure could be occurring under ambient conditions if illite or similarly weak minerals are distributed along optimally oriented preexisting normal faults, as discussed in more detail below.

2.2 Fracture Geometry in Stimulation Interval

Davatzes and Hickman (2009) analyzed borehole televiewer (BHTV) and Formation MicroScanner (FMS) image logs to determine the orientation and depth distribution of natural fractures and bedding or foliation throughout well 27-15. In their analysis, natural fractures were differentiated from bedding/foliation on the basis of the latter exhibiting closely spaced, sub-parallel traces of uniform acoustic reflectivity and resistivity contrast with the borehole wall. Conservative picking by Davatzes and Hickman probably underestimated the total number of fractures in well 27-15, but leads to a more reliable analysis of structure orientation and distribution. In Figures 4b and c, we show the orientations of natural fractures determined for the entire well and for the planned stimulation interval from the BHTV and FMS logs. In this and all figures, azimuths of features in the image logs have been corrected for deviation of the borehole from vertical and corrected to true north.

Davatzes and Hickman (2009) also determined the orientation of the horizontal principal stresses in well 27-15 through analysis of drilling-induced tensile fractures seen in both the BHTV and FMS logs. The mean orientation of S_{hmin} was calculated by averaging the orientation of drilling-induced tensile fractures

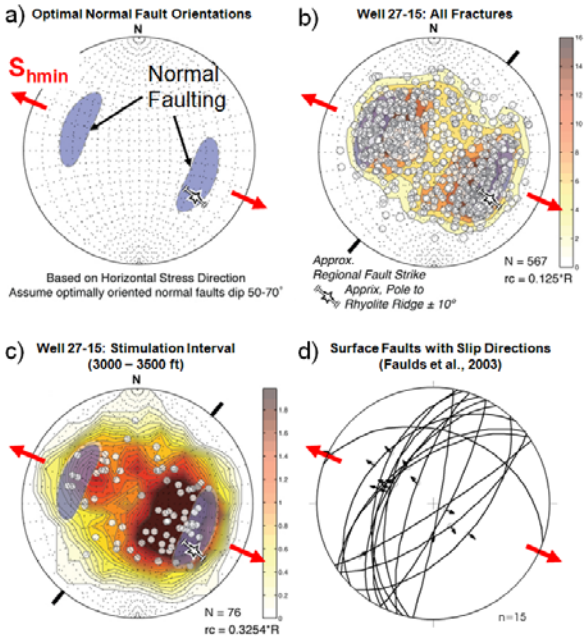

Figure 4: Lower hemisphere, equal area stereographic projections showing stress directions and poles to natural fractures from analysis of image logs by Davatzes and Hickman (2009). a) The blue shaded areas in each figure indicate poles to planes that are well oriented for normal faulting given the current direction of S_{hmin} (114 ± 17°, red arrows). Poles to fractures (open circles) and contours to poles (shaded in color) are shown for b) the entire well and c) the planned stimulation interval. d) Great circle representations of faults mapped in the Hot Springs Mountains (Figure 1) by Faulds and Garside (2003), with black arrows indicating slip directions inferred from fault striations (e.g., slickenlines) and other kinematic indicators.

weighted by their lengths. In this manner, they determined that S_{hmin} in well 27-15 is oriented 114 ± 17°, which can be used to predict the orientation of natural fractures that would be well oriented for conjugate normal faulting (shaded regions in Figure 4a). Previous analysis by Robertson-Tait et al. (2004) of stress directions from borehole failure observed in well 23-1, located 1.3 miles E-SE of well 27-15, is in excellent agreement with stress orientations from well 27-15 (Figure 1).

Significant sub-populations of fractures imaged both over the entire open-hole interval of well 27-15 (Figure 4b) and within the planned EGS stimulation interval (Figure 4c) are well oriented for normal faulting given the current orientation of S_{hmin}. This stress orientation is also consistent with normal slip on a set of ESE and WNW dipping normal faults inferred from seismic reflection surveys (Lutz et al., 2009) and mapped at the surface by Faulds and Garside (2003; Figure 1, also shown as black tic marks and star in Figures 4b and c). In particular, the orientations of surface faults mapped in the Hot Springs Mountains (Figure 1) by Faulds and Garside (2003) and the slip directions inferred on these faults from fault striations and other kinematic indicators are remarkably similar to down-dip slip directions expected on these faults for a simple normal faulting stress regime, given the current orientation of S_{hmin} (Figure 4d).

2.3 Three-Dimensional Stress Model

In order to calculate the propensity for frictional failure on fractures seen in the stimulation interval (Figure 4c), as needed for stimulation planning, requires constraints on the magnitudes and orientations of all three principal stresses. For the magnitude of S_{hmin} and S_V we used results from the minifrac and overburden calculations discussed above (Figure 3), with S_{hmin} extrapolated over the stimulation interval assuming a constant ratio S_{hmin}/S_V. For horizontal stress directions we used the mean azimuth of S_{hmin} as determined for well 27-15 by Davatzes and Hickman (2009; see Figure 4).

The magnitude of the remaining principal stress, S_{HMax}, can either be bounded by tectonic considerations or constrained directly through observations and modeling of stress-induced borehole failure (i.e., breakouts and tensile fractures). As discussed in Davatzes and Hickman (2009), based upon the poor quality of image logs in this highly washed-out well, it was not possible to ascertain with confidence whether or not breakouts occurred in this well. Thus, we could not use observations of breakouts in conjunction with rock strength constraints as used in other geothermal studies to constrain the magnitude of S_{HMax} (e.g., Hickman et al., 1998; Davatzes and Hickman, 2006).

Instead, in our geomechanical analysis we place bounds on S_{Hmax} using two stress models. The first model assumes a typical normal faulting stress environment in which S_{Hmax} is midway between S_{hmin} and S_V, i.e., $S_{Hmax} = (S_{hmin} + S_V)/2$. This model (termed the NF model) is consistent both with the regional tectonic style of the western Basin and Range province (Zoback, 1989; Heidbach, 2008) and with the observation that slip directions on nearby faults mapped at the surface are down-dip and parallel to S_{hmin} (Figures 1 and 4d). The second model assumes that S_{Hmax} and S_V are equal in magnitude, which corresponds to a transitional normal faulting to strike-slip stress regime, i.e., $S_{Hmax} = S_V$. Since there are no reported active strike-slip faults in this area, this second model (termed the NF/SS model) provides a reasonable upper bound to the magnitude of S_{Hmax}. The magnitudes of S_{Hmax} corresponding to these two stress models at the minifrac depth are shown in Figure 3.

2.4 Geomechanical Analysis

As for most EGS projects (MIT, 2006), the preferred strategy for the stimulation of well 27-15 is to generate self-propping shear failure at fluid pressures less than S_{hmin}. Although higher fluid pressures can be used if necessary, pressures in excess of S_{hmin} would generate a massive hydraulic fracture, possibly leading to uncontrolled vertical fracture growth and high fluid losses into the lower-temperature cap rock and smectite alteration zone behind the casing (see Figure 3). Based upon the results of the minifrac test discussed above and assuming formation water in the borehole at ambient temperatures, this places an upper bound on stimulation pressures of ~750 psi at the wellhead before a hydraulic fracture would be initiated at the top of the stimulation interval (HFP labeled in Figure 3). With this in mind, the following analyses were carried out to predict excess fluid pressures required to generate self-propping shear failure while staying below the least principal stress, S_{hmin}. Although fluid pressures in the ensuing analysis are presented in terms of wellhead pressures under ambient borehole conditions, during stimulation of well 27-15 these pressures will be adjusted based upon down-hole pressure recording to account for wellbore cooling during fluid injection.

Using the NF and NF/SS stress models, conditions necessary to induce frictional failure on pre-existing natural fractures in the stimulation interval of well 27-15 can be calculated. In accord with the Coulomb failure criteria (e.g., Jaeger and Cook, 1976), frictional sliding will occur along a fracture with

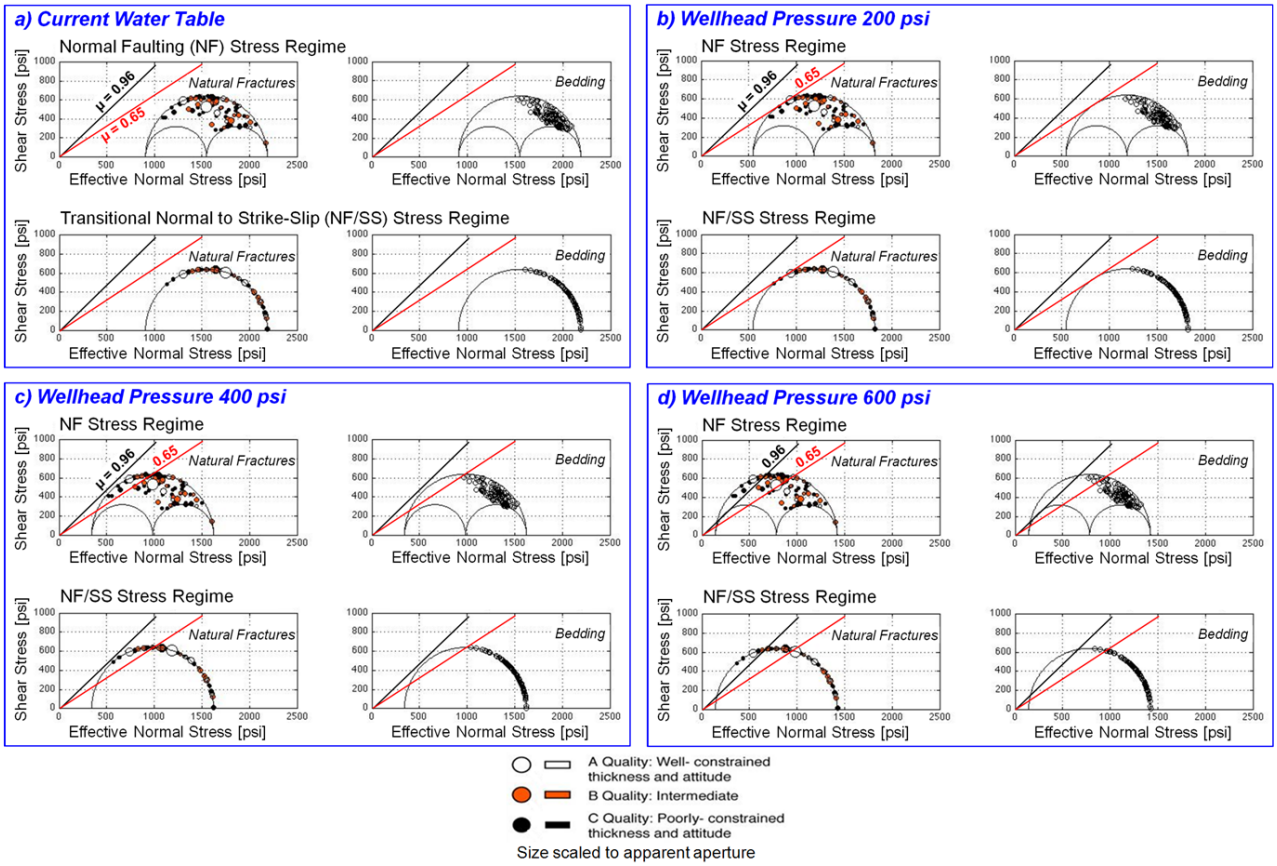

Figure 5: Three-dimensional Mohr circles showing shear and effective normal stresses resolved onto fractures and bedding planes (or foliation) seen in the electrical and acoustic image logs in the planned EGS stimulation interval for Well 27-15 (~3000 to 3500 ft). Plots are for two end-member stress regimes − normal faulting or transitional normal to strike-slip faulting − under different hydraulic stimulation scenarios: a)formation fluid pressure in equilibrium with the current water table (undisturbed background case) and formation fluid pressures in equilibrium with excess wellhead pressures of b) 200 psi, c) 400 psi and d) 600 psi. Also shown are frictional failure lines (Equation 2) corresponding to coefficients of sliding friction, μ, of 0.65 to 0.96, as derived from laboratory testing on core from nearby well 35-13 (see text). The color code shown corresponds to the quality of the fracture images obtained, with symbol size proportional to apparent fracture aperture.

friction coefficient μ and internal fluid pressure P_P at a critical shear stress, τ_{crit}, given by:

$$|\tau| = \tau_{crit} = \mu(\sigma_N - P_P) + S \qquad (2)$$

where τ and σ_N are the shear and normal stresses, respectively, resolved onto that fracture and S is the cohesion. As in the preceding analysis (Equation 1), these fracture planes were assumed to be cohesionless (i.e., S = 0), which is supported by in-situ stress measurements in a variety of tectonically active geologic settings (see reviews by Hickman, 1991, and Townend and Zoback, 2000). The shear stress and effective normal stress (i.e., $\sigma_N - P_P$) acting on each fracture plane seen in the stimulation interval was computed knowing the principal stress magnitudes and the orientation of the fracture plane with respect to the principal stress axes, for a range of assumed values for P_P (see Jaeger and Cook, 1976). The results of this analysis are depicted as 3D Mohr diagrams of shear stress versus effective normal stress, where each symbol corresponds to an individual fracture mapped using image logs in the stimulation interval (Figure 5). In this plot we also show shear and effective normal stress resolved onto bedding (or foliation) planes in the stimulation interval.

Four different fluid pressure scenarios were considered in this analysis, corresponding to P_p at its current ambient level (with water table at 380 ft GL), and P_p for wellhead pressures of 200 psi, 400 psi and 600 psi (Figure 5). These pressures were chosen not to exceed the wellhead hydrofrac pressure of ~750 psi (Figure 3). In translating wellhead pressure to excess formation fluid pressure for these calculations, it is assumed that formation fluid fills the borehole and that borehole temperatures are in equilibrium

with ambient formation temperatures. In this case, excess formation pressure can be obtained by adding 165 psi to the wellhead pressures shown in Figure 5. As mentioned above, injection will cool the borehole to varying degrees and downhole pressure sensors will be used to monitor excess formation pressure at the borehole wall during stimulation of well 27-15.

Frictional failure lines corresponding to Equation 2 are superimposed on the Mohr circles in Figure 5, using coefficients of sliding friction derived from triaxial laboratory testing of cores from well 35-13 under realistic in-situ effective confining pressures (Table 4 in Lutz et al, 2010). These cores were selected as being most representative of lithologies encountered in the stimulation interval of well 27-15. These μ values were derived at the conclusion of each test, after a thoroughgoing fracture had formed and the fractures were sliding under quasi-steady-state conditions, and generally ranged from 0.65 to 0.96 (plotted in Figure 5). The one exception to this is an outlying value of μ = 1.215, which was derived from a metamorphosed mudstone based on testing at only two confining pressures; this value is unrealistically high for sliding friction (see Lockner and Beeler, 2002) and was not used in this analysis. The small residual cohesion values from these sliding friction tests were neglected in this analysis, since (as noted by Lutz et al., 2010) they likely reflect the strength of jacket material used to enclose samples during testing and are not a real rock property.

3. DISCUSSION

At current fluid pressures, analysis of the propensity for frictional failure shows that both natural fractures and bedding/foliation should be frictionally stable within the planned stimulation interval, for either a NF or NF/SS stress regime (Figure 5a). This agrees with the previous observation that differential stress (S_V - S_{hmin}) at this location is too low to result in pervasive frictional failure on optimally oriented normal faults for typical laboratory friction values (Figure 3). However, as the ambient water level in well 27-15 is raised and wellhead pressures increased from 200 to 400 and finally to 600 psi, this analysis shows that more and more fractures within the stimulation interval fall within the frictional failure envelope bounded by the lines for μ= 0.65 and 0.96 (Figures 5 b, c and d). By the time a wellhead pressure of 600 psi is reached, a significant number of the natural fractures within the stimulation interval fall within or beyond this failure envelope (Figure 5d), suggesting widespread frictional failure. By plotting the ratio of shear to effective normal stress on fractures as a function of depth for a wellhead pressure of 600 psi, it can be seen that the greatest density of fractures with a high tendency for slip (especially large-aperture fractures) exists within the siliceous rhyolites above about 3300 ft GL (Figure 6). Note that very few of the bedding or foliation planes within the stimulation interval should be triggered into failure by raising wellhead fluid pressure, except at the highest pressures of 600 psi (Figure 5d). This is not surprising given the generally lower dip angles of bedding/foliation when compared to fractures in this interval (Davatzes and Hickman, 2009).

Although sliding friction measurements on rocks representative of the stimulation interval indicate high μ of 0.65 to 0.96, illite and related clays (illite + mica, illite/smectite) constituted ~15 to 40% of the cuttings analyzed with XRD from the well 27-15 stimulation interval (Lutz et al, 2010). Since μ ~0.45 for illite (Lockner and Beeler, 2002), as noted above (Figure 3) it is possible that frictional failure might be induced at lower fluid pressures than indicated in Figure 5, but only if significant quantities of illite or other weak clays were present as contiguous linings along natural fractures within the stimulation interval. Even so, as discussed by Lutz et al. (2010) frictional failure along relatively soft/ductile clay minerals would not be expected to result in significant fracture dilatation and permeability enhancement (see also discussion in Davatzes and Hickman, 2005). Thus, use of the higher, "hard rock" friction values derived by Lutz et al. (2010) and used in the analyses presented in Figure 5 is more appropriate for predicting the onset of shear-induced dilatation and permeability enhancement during EGS stimulation of well 27-15.

In concert with other hydrological, geochemical and structural considerations, the preceding analysis was used by the Desert Peak EGS Team to design the overall stimulation strategy for well 27-15, which will consist of the following general phases (see also Zemach et al., 2009):

1. Conduct initial hydraulic stimulation, increasing wellhead pressure in steps to 600 psi, to induce shear failure while staying below S_{hmin} (Figures 3 and 5). Inject tracers during stimulation and sample at nearby producers to gauge stimulation effectiveness.
2. If necessary, conduct chemical stimulation to preferentially dissolve fracture and vein fillings. Analyze flow-back fluid, and then conduct additional shear stimulation at pressures < S_{hmin}.
3. If necessary, conduct hydraulic fracturing at wellhead pressures in excess of S_{hmin} (Figure 3) to break down the formation near the borehole, followed by additional shear stimulation.

These phases will be monitored with a 14 station seismic array deployed around Desert Peak well 27-15 by the U.S. Geological Survey and Lawrence Berkeley National Laboratory, to track the progress of the stimulation using microearthquake locations.

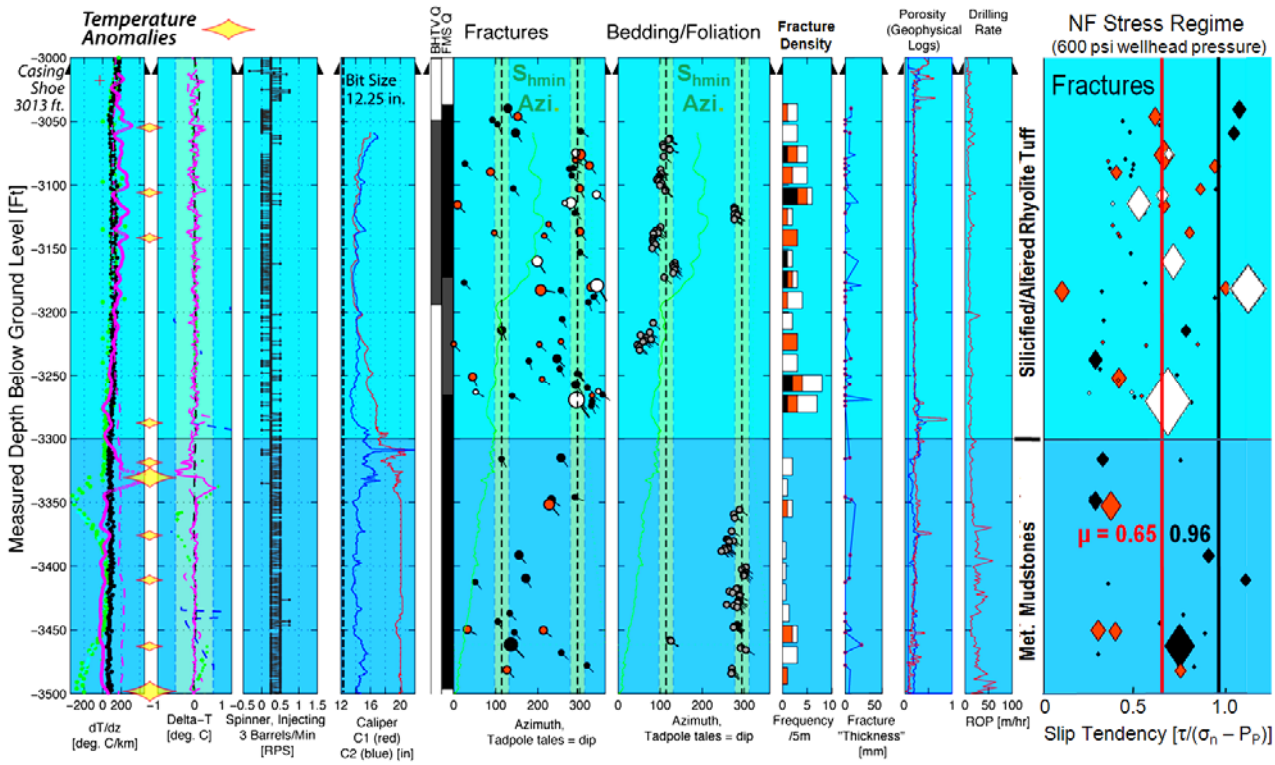

Figure 6: Compilation of well log data and analyses over the EGS stimulation interval for well 27-15. Detailed analysis of drill cuttings by Lutz et al. (2010) shows that the stimulation interval consists of either silicified and altered rhyolite tuffs (light blue) or metamorphosed hematitic mudstones (dark blue). From left to right:

- *Temperature logs. Analysis of the logs includes filtering and smoothing to remove measurement artifacts or improve temperature resolution (see Davatzes and Hickman, 2009, for details). Data presented are:*
  - *(1) Temperature gradient*
  - *(2) Differential temperature (delta T)*
  - *(3) Identified permeable zones (yellow diamonds)*
- *Spinner flow meter log during fluid injection at 2.75 bbl/min while logging down at 30 ft/min.*
- *Four-arm caliper log, compared to the nominal bit size in the open-hole interval (12.25 inches)*
- *Quality of the borehole televiewer (BHTV) and Formation MicroScanner (FMS) image logs, with black, dark grey, light grey and white corresponding to best, good-to-fair, poor and unusable quality, respectively.*
- *Tadpole plot showing natural fracture dip direction versus depth from the image logs. The head of the tadpole indicates dip azimuth and angle of the tadpole tail (relative to horizontal) indicates dip of the fracture plane. The colors of the tadpoles reflect the quality of the pick, using the scale shown in Figure 5. Also plotted are:*
  - *(1) Borehole deviation direction (green line).*
  - *(2) Direction of S_{hmin} ± 1 standard deviation: 114±17° (vertical black dashed lines and green regions).*
- *Tadpole plot showing bedding or foliation dip from the image logs.*
- *Natural fracture density per 5 m bins, color coded by image log quality.*
- *Natural fracture apparent aperture, or thickness, in the image logs.*
- *Porosity derived from wireline geophysical logs, using sonic velocity (blue) and density (red).*
- *Rate of penetration during drilling.*
- *Tendency for frictional failure on individual fractures seen in the image logs under a wellhead pressure of 600 psi, expressed as the ratio of shear to effective normal stress. Color code corresponds to the quality of the fracture images (see key in Figure 5), with symbol size proportional to apparent fracture aperture. Also shown are frictional failure lines corresponding to coefficients of friction, μ, ranging from 0.65 to 0.96, as measured by Lutz et al. (2010) on core samples from well 35-13 that are representative of lithologies encountered in the stimulation interval for well 27-15.*

This network will also provide additional useful constraints for comparison with the 3-dimensional stress and geomechanical models presented above, by allowing determination of earthquake focal mechanisms and the relative roles of shear *vs.* dilatational failure during the stimulation. In addition, injection testing, TPS and image logging, and tracer testing will be conducted before and after all phases of the stimulation, to diagnose changes in reservoir hydrologic properties and identify the distribution and orientation of permeable fractures.

For a successful EGS hydraulic stimulation, the formations being targeted should have the appropriate mechanical properties to result in "self-propping" dilatation and permeability enhancement during shearing. Mechanical testing, microstructural observations and theoretical considerations suggest that harder (i.e., higher compressive strength, higher Young's modulus) rocks with lower porosity and lower clay content are more likely to experience persistent permeability enhancement following shearing under high effective normal or confining stresses (Wong and Zhu, 1999; Crawford et al., 1999; Davatzes and Hickman, 2005; Cipolla et al., 2008).

As discussed in detail by Lutz et al. (2010), the planned stimulation interval for well 27-15 consists of two distinctly different rock types: an upper stimulation zone (~3000 to 3300 ft GL) comprised of silicified and altered rhyolite tuffs and a lower stimulation zone (~3300 to 3500 ft GL) comprised of metamorphosed hematitic mudstones (Figure 6). Lutz et al. (2010) conducted mechanical testing on cores of siliceous rhyolite tuff from well 35-13, which is representative of most of the upper stimulation zone from well 27-15. Tests on four samples from this lithology show that the quasi-static Young's modulus ranges from 3.20×10^6 to 3.84×10^6 psi. Although, cores are not available that were as closely representative of the lower stimulation zone, mechanical testing was conducted on cores of illitic/siliceous metamudstones from well 35-13 that are similar in fabric and composition (but poorer in hematite) to the lower stimulation zone of well 27-15 (S. Lutz, pers. comm., 2010). Tests on two samples from this lithology indicate quasi-static Young's modulus values of 4.40×10^6 and 5.52×10^6 psi. Based upon laboratory testing of fractured rock and using theoretical extrapolations, Cipolla et al. (2008) show that for shear fractures to be self-propping and remain open under ambient effective normal stresses appropriate to the well 27-15 stimulation interval (~1000 to 2000 psi; Figure 5a), these rocks have to have a Young's modulus of $\sim 1 \times 10^6$ psi or greater. Since the Young's modulus appropriate to the well 27-15 stimulation interval is about 3 to 6 times greater than this threshold value, the prognosis for creation of persistent, self-propping shear failure during hydraulic stimulation of well 27-15 is good.

This conclusion is supported by X-ray computed tomography (CT) scans and gas permeability measurements conducted before and after shearing on the rhyolite tuff cores from well 35-13 (Lutz et al., 2010). These measurements show generation of significant interconnected porosity and up to a 20-fold increase in permeability along fractures sheared at stresses and fluid pressures relevant to the planned EGS stimulation of well 27-15. Thus, although similar testing has not been performed on the hematitic mudstones appropriate to the lower stimulation zone, the lab results of Lutz et al. (2010) also bode well for the success of shear-enhanced permeability creation during hydraulic stimulation of well 27-15.

The lower stimulation zone has a generally higher clay content than the upper zone (Lutz et al., 2010), suggesting on purely mineralogical grounds that it might be less conducive to shear-induced dilatation. This is consistent with the observation that the borehole diameter is much more enlarged in the lower zone, suggesting weaker rock in situ, and that both the rate of penetration during drilling and (to a lesser extent) the geophysically inferred porosities are higher and more variable in the lower zone (Figure 6). However, this interpretation is not supported by analyses of core samples from well 35-13, which show comparable values both for Young's modulus (discussed above) and for unconfined compressive strengths from strength profiling ("scratch" tests; Lutz et al., 2010) for rock types representative of both zones. Whether or not one of these two zones is most conducive to shear-enhanced dilatation will not be known until detailed hydrologic testing and borehole logging is carried out following hydraulic stimulation.

Davatzes and Hickman (2009) compared static equilibrated and non-equilibrated temperature logs conducted in well 27-15 prior to the July 2009 recompletion to identify flow zones that are connected to the larger-scale formation permeability. In Figure 6, we show the results of this analysis for the planned stimulation interval, wherein persistent temperature anomalies, identified through analysis of temperature gradients and differential temperatures, are shown as yellow diamonds. The most prominent of these permeable zones are at depths of 3330 ft and 3497 ft, with the latter zone identified on the basis of a temperature anomaly that is just off scale in this figure (see Davatzes and Hickman, 2009). These anomalies are not expressed or are only slightly expressed in the spinner response, which indicates that they contribute little to the overall injectivity of this interval, which is quite low. Minor temperature anomalies (smaller diamonds) are seen at numerous other depths. These temperature anomalies − both large and small − indicate that there are numerous

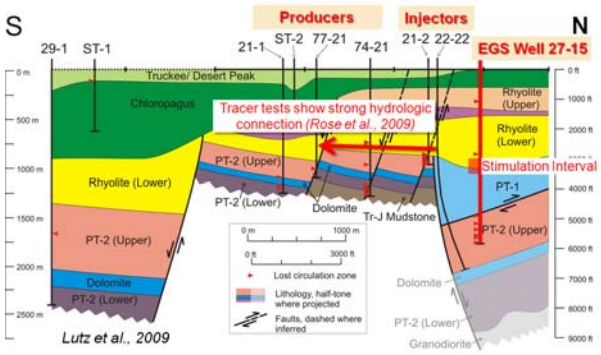

Figure 7: Interpreted south-to-north cross section through the Desert Peak Geothermal Field (modified from Lutz et al., 2009). EGS well 27-15 and the locations of currently active production and injection wells are highlighted (see Figure 1). The planned stimulation interval in well 27-15 is at depths of ~3000 to 3500 ft, at the base of the Tertiary Rhyolites and at the top of the pre-Tertiary metasedimentary rocks (PT-1). The red arrow illustrates the strong hydrologic connection that exists between injecting wells immediately to the south of well 27-15 (i.e., wells 21-2 and 22-22) and producing wells in the main part of the geothermal field (Rose et al., 2009).

fluid loss zones within the stimulation interval that could form good exit points for fluid during low-pressure stimulation. However, these anomalies are fairly spread out and are not easily correlated with specific fractures seen in the image logs.

Previous studies in normal faulting and strike-slip faulting stress environments show that shear fracture formation during hydraulic stimulation tends to be aligned in the direction of S_{Hmax}, even at injection pressures considerably less than the least principal stress. This tendency for permeability growth to align with S_{Hmax} has been observed in oil and gas fields based upon preferential directions of water flood "breakthrough" between wells and microseismic monitoring, whether or not those fields are considered to be fracture dominated (Heffer et al., 1995; Willis-Richards et al., 1996; Heffer, 2002; Rahman et al., 2002). Similarly, the microseismic clouds produced during hydraulic stimulation of Soultz-sous-Forêts, France, geothermal wells GPK2, GPK3 and GPK4 at pressures less than the least principal stress were also aligned in the direction of S_{Hmax} (e.g., Schindler et al., 2008; Valley and Evans, 2007). Thus, in the case of well 27-15, we expect the enhanced permeability zone to be created during EGS hydraulic stimulation to grow preferentially parallel to S_{Hmax}, in a SSW direction toward nearby injection and production wells, or to the NNE, toward an undeveloped part of the field (Figure 1). This directionality makes sense on a mechanistic level, since this anticipated growth direction is parallel to the strike of optimally oriented, conjugate normal faults observed throughout the well and within the stimulation interval (Figure 4). These fractures should link up and promote fracture connectivity along their common strike direction in response to down-dip shearing during hydraulic stimulation.

Importantly, tracer tests (Rose et al., 2009) indicate that a strong hydrologic connection already exists through the base of the rhyolites between the injector wells immediately south of well 27-15 and producing wells in the main part of the geothermal field (Figure 7). Thus, to improve the hydrologic connection between well 27-15 and the northern end of the currently active field, the permeability enhanced zone generated during hydraulic stimulation of well 27-15 has to propagate a distance of ~1500 ft or less, depending on the spatial extent of high permeabilities associated with wells 21-2 and 22-22. Indeed, stimulated volumes with more than this lateral extent have been created in other EGS projects, such as in a NF/SS stress regime at Soultz-sous-Forêts (e.g., Schindler et al., 2008) and in a reverse faulting stress regime in the Cooper Basin, Australia (Asanuma et al., 2009). If the stimulation of well 27-15 is successful, then it could greatly enhance the hydraulic connectivity between well 27-15 and the currently active geothermal field to the SSW, facilitating utilization of well 27-15 either as an injection or a production well (see Zemach et al., 2009).

4. CONCLUSIONS

The interval selected for hydraulic stimulation in Desert Peak EGS well 27-15 (depth ~3000 to 3500 ft) contains numerous natural fractures that are well-oriented for normal faulting in the present stress field. Even though the injectivity of this interval is quite low, slightly permeable fractures accessible to hydraulic stimulation are present at multiple depths.

A mini hydraulic fracturing test conducted in well 27-15 at a depth of 3054 ± 41 ft GL indicates that the magnitude of the least horizontal principal stress, S_{hmin}, is 1995 ± 60 psi. This is ~0.61 of the calculated vertical stress at this depth, and places an upper bound on well-head pressures to be used during shear hydraulic stimulation of ~750 psi. Pressures in excess of this could lead to uncontrolled vertical growth of massive hydraulic fractures, with resultant loss of fluids into the overlying, lower-temperature cap rock.

A Coulomb failure analysis was conducted of the propensity for frictional failure on pre-existing natural fractures seen in the stimulation interval for two end-member stress models: pure normal faulting and transitional normal to strike-slip faulting. This

analysis, which used sliding friction coefficients measured on representative drill cores from a nearby well, indicates that frictional failure should be induced on pre-existing factures in the stimulation interval starting at wellhead pressures of ~200 psi, corresponding to excess formation pressures of ~365 psi. This result is now being used to help plan the EGS stimulation for well 27-15, in concert with other members of the Desert Peak EGS Project Team.

The direction of S_{Hmax} from observations of drilling-induced tensile cracks in well 27-15 is 24 ± 17º, which is parallel to the strike of conjugate normal faults in this well that are susceptible to frictional failure during hydraulic stimulation. This stress direction should preferentially drive shear stimulation and permeability growth from EGS well 27-15 toward injecting wells located ~1500 ft to the SSW, which are known from tracer tests to be well connected to the main producing part of the Desert Peak Geothermal Field (Rose et al., 2009).

Comparison of elastic properties measured on representative core samples from Desert Peak well 35-13 with criteria for creation of self-propping shear fractures in oil and gas fields suggests that rocks within the stimulation interval for well 27-15 are mechanically strong enough to generate and maintain significant fracture permeability upon shearing. This conclusion is supported by pre- and post-failure X-ray (CT) scanning and permeability measurements on these same rock units by Lutz et al. (2010), which demonstrate significant fracture dilatation and permeability creation during shearing. Thus, the prospects for a successful EGS hydraulic stimulation of Desert Peak Well 27-15 are high.

5. ACKNOWLEDGMENTS

We acknowledge collaboration and support from Ormat Technologies, Inc., that made this research possible, in particular Ezra Zemach, Peter Drakos, Mark Tibbs, Terry Crowson, Gene Suemnicht and Stuart Johnson. We also thank Joe Svitek of the USGS for maintaining and operating the logging truck, tools and other field equipment associated with this operation and Joe Henfling, Dennis King and Douglas Blankenship of Sandia National Lab for their support in televiewer operations, maintenance and modification. This work benefitted from scientific discussions with Ann Robertson-Tait, Peter Rose, Susan Lutz and Colin Williams. The Desert Peak EGS project is supported by the U.S. Department of Energy, Assistant Secretary for Energy Efficiency and Renewable Energy, under DOE Grant No. DE-FC36-02ID14406 with additional support provided by the USGS Energy Resources Program.

6. REFERENCES

Asanuma, H., Kenmoku, Y., Niitsuma, H., and Wyborn, D. (2009), Interpretation of reservoir creation process at Cooper Basin by microseismic multiplet analysis, *Geothermal Resources Council Transactions*, v. 33, p. 149-153.

Barton, C.A., Zoback, M.D., and Moos, D. (1995), Fluid flow along potentially active faults in crystalline rock, *Geology*, v. 23, no. 8, p. 683-686.

Barton, C., Hickman, S., Morin, R., Zoback, M.D., and Benoit, R. (1998), Reservoir-scale fracture permeability in the Dixie Valley, Nevada, geothermal field, *in* Holt, R. M. et al. (eds.), *Rock Mechanics in Petroleum Engineering*, v. 2, Richardson, TX, Society of Petroleum Engineers, p. 315-322.

Byerlee, J.D. (1978), Friction of rocks, *Pure and Applied Geophysics*, v. 116, p. 615-629.

Cipolla, C.L., Warpinski, N.R., Mayenhofer, M.J., and Lolon, E.P. (2008), The relationship between fracture complexity, reservoir properties and fracture treatment design, *SPE Annual Technical Conference and Exhibition*, Denver, CO, Sept. 21-24, 2008, SPE paper 115769.

Crawford, B., Hutcheon, R., Smart, B. and Yale, D. (1999), Coupled Mechanical Deformation and Fluid Flow in Experimentally Yielded Granular Reservoir Materials, in Vouille, G. and Berest, P. (eds.) *Proceedings of the 9th International Congress on Rock Mechanics*, 25-28 August 1999, Paris, France, Rotterdam, A.A. Balkema.

Davatzes, N.C. and Hickman, S. (2005), Controls on fault-hosted fluid flow: Preliminary results from the Coso Geothermal Field, CA, *Geothermal Resources Council Transactions*, v. 29, p. 343-348.

Davatzes, N.C, and Hickman, S. (2006), Stress and faulting in the Coso Geothermal Field: Update and recent results from the East Flank and Coso Wash, *Proceedings 31st Workshop on Geothermal Reservoir Engineering*, Stanford Univ., Stanford, CA, SGP-TR-179.

Davatzes, N.C. and Hickman, S. (2009), Fractures, stress and fluid flow prior to stimulation of well 27-15, Desert Peak, Nevada, EGS Project, *Proceedings 34th Workshop on Geothermal Reservoir Engineering*, Stanford Univ., Stanford, CA, SGP-TR-187.

Faulds, J.E., and Garside, L.J. (2003), Preliminary geologic map of the Desert Peak – Brady geothermal fields, Churchill County, Nevada, *Nevada Bureau of Mines and Geology Open-File Report 03-27*.

Heffer, K. (2002), Geomechanical Influences in Water Injection Projects: An Overview, *Oil and Gas Science and Technology*, v. 57, No. 5, p. 415-422.

Heffer, K.J., Fox, R.J., McGill, C.A., and Koutsabeloulis, N.C. (1995), Novel Techniques Show Links between Reservoir Flow Directionality, Earth Stress, Fault Structure and Geomechanical Changes in Mature Waterfloods, *Presented at SPE Annual Technical Conference and Exhibition, Dallas TX*, 22-25 October, 1995, SPE paper 30711.

Heidbach, O., Tingay, M., Barth, A., Reinecker, J., Kurfeß, D., and Müller, B. (2008), The World Stress Map database release 2008 doi:10.1594/GFZ.WSM.Rel2008.

Hickman, S. (1991), Stress in the lithosphere and the strength of active faults, *U.S. National Report to the International Union of Geodesy and Geophysics 1987-1990, Reviews of Geophysics*, v. 29, p. 759-775.

Hickman, S., and Zoback, M.D. (1983), The interpretation of hydraulic fracturing pressure-time data for in-situ stress determination, in *Hydraulic Fracturing Measurements*, edited by M.D., Zoback and B.C. Haimson, National Academy Press, Washington, D.C., p. 44-54.

Hickman, S.H., Zoback, M.D., and Healy J.H. (1988), Continuation of a deep borehole stress measurement profile near the San Andreas Fault, I: Hydraulic fracturing stress measurements at Hi Vista, Mojave Desert, California, *Journal of Geophysical Research*, v. 93, p. 15183-15195.

Hickman, S., Zoback, M.D., Benoit, R. (1998), Tectonic controls on fault-zone permeability in a geothermal reservoir at Dixie Valley, Nevada, in *Rock Mechanics in Petroleum Engineering, v. 1*, R. M. Holt et al. (eds.), Soc. Petroleum Eng., Richardson, TX., p. 79-86.

Hickman, S., Zoback, M.D., Barton, C., Benoit, R., Svitek, J. and Summers, R. (2000), Stress and permeability heterogeneity within the Dixie Valley geothermal reservoir: Recent results from well 82-5, *Proceedings 25th Workshop on Geothermal Reservoir Engineering*, Stanford Univ., Stanford, CA, p. 256-265.

Ito, T. and Zoback, M.D. (2000), Fracture permeability and in situ stress to 7 km depth in the KTB scientific drillhole, *Geophysical Research Letters*, v. 27, p. 1045-1048.

Jaeger, J.C., and Cook, N.G. (1976), *Fundamentals of Rock Mechanics*, 2nd ed., Chapman and Hall, London, 585 pp.

Lockner, D.A., and Beeler, N.M. (2002), Rock failure and earthquakes, in *International Handbook of Earthquake and Engineering Seismology*, Chapter 32, edited by W.. Lee, H. Kanamori, P. Jennings and C. Kisslinger, Academic Press, Amsterdam, p. 505-537.

Lutz, S., Moore, J., Jones, C., Suemnicht, G., and Robertson-Tait, A. (2009), Geological and structural relationships in the Desert Peak Geothermal System, Nevada: Implications for EGS development, *Proceedings 34th Workshop on Geothermal Reservoir Engineering*, Stanford Univ., Stanford, CA, SGP-TR-187.

Lutz, S.L., Hickman, S., Davatzes, N., Zemach, E., Drakos, P., and Robertson-Tait, A. (2010), Rock mechanical testing and petrologic analysis in support of well stimulation activities at the Desert Peak Geothermal Field, Nevada, *Proceedings 35th Workshop on Geothermal Reservoir Engineering*, Stanford Univ., Stanford, CA, SGP-TR-188.

MIT (2006), *The future of geothermal energy: Impact of enhanced geothermal systems (EGS) on the United States in the 21st century*, Cambridge, MA, Massachusetts Institute of Technology.

Rahman, M.K., Hossain, M.M., and Rahman, S.S. (2002), A shear-dilation-based model for evaluation of hydraulically stimulated naturally fractured reservoirs, *International Journal For Numerical and Analytical Methods in Geomechanics*, v. 26, p. 469-497.

Robertson-Tait, A., Lutz, S.J., Sheridan, J., and Morris, C.L. (2004), Selection of an interval for massive hydraulic stimulation in well DP 23-1, Desert Peak East EGS project, Nevada, *Proceedings, 29th Workshop on Geothermal Reservoir Engineering*, Stanford University, Stanford CA, SGP-TR-175.

Rose, P., Leecaster, K., Drakos, P., and Robertson-Tait, A. (2009), Tracer testing at the Desert Peak EGS Project, *Geothermal Resources Council Transactions*, v. 33, p. 241-244.

Schindler, M., Nami, P., Schellschmidt, R., Teza, D., and Tischner, T. (2008), Summary of hydraulic stimulation operations in the 5-km-deep crystalline HDR/EGS reservoir at Soultz-sous-Forêts, *Proceedings, 33rd Workshop on Geothermal Reservoir Engineering*, Stanford University, Stanford CA, SGP-TR-185.

Townend, J., and Zoback, M. D. (2000), How faulting keeps the crust strong. *Geology*, v. 28, p. 399–402.

Valley, B., and Evans, K.F. (2007), Stress state at Soultz-sous-Forêts to 5 km depth from wellbore failure and hydraulic observations, *Proceedings, 32nd Workshop on Geothermal Reservoir*

Engineering, Stanford University, Stanford CA, SGP-TR-183.

Willis-Richards, J., Watanabe, K., and Takahashi, H. (1996), Progress toward a stochastic rock mechanics model of engineered geothermal systems, *Journal Geophysical Research*, v. 101, p. 17481-17469.

Wong, T.-f., and Zhu, W. (1999), Brittle faulting and permeability evolution: Hydromechanical measurement, microstructural observation and network modeling, *AGU Geophysical Monograph,* v. 113, p. 83-99.

Zemach, E., Drakos, P., and Robertson-Tait, A. (2009), Feasibility evaluation of an "in-field" EGS project at Desert Peak, Nevada, *Geothermal Resources Council Transactions*, v. 33, p. 285-295.

Zoback, M.D. (2007), *Reservoir Geomechanics*, Cambridge Univ. Press, New York, 449 pp.

Zoback, M. L. (1989), State of stress and modern deformation of the northern Basin and Range Province, *Journal of Geophysical Research*, v. 94, p. 7105-7128.